

Article

Ascorbic Acid Sensor Based on CdS QDs@PDA Fluorescence Resonance Energy Transfer

Pu Li ¹, Xiaoxiao Chen ¹, Gaojun Wu ², Zhe Wang ² and Chaobiao Huang ^{1,2,*}

¹ College of Chemistry and Life Science, Zhejiang Normal University, Jinhua 321004, China; 202020200588@zjnu.edu.cn (P.L.); 26947255692@zjnu.edu.cn (X.C.)

² Xingzhi College, Zhejiang Normal University, Jinhua 321004, China; 202120200767@zjnu.edu.cn (G.W.); L15839984772@163.com (Z.W.)

* Correspondence: hcb@zjnu.cn

Abstract: An ascorbic acid (AA) sensor was constructed based on the fluorescence resonance energy transfer (FRET) between CdS quantum dots (CdS QDs) and polydopamine (PDA) to detect trace AA sensitively. FRET occurred due to the broad absorption spectrum of PDA completely overlapped with the narrow emission spectrum of CdS QDs. The fluorescence of CdS QDs was quenched and in the “off” state. When AA was present, the conversion of DA to PDA was hindered and the FRET disappeared, resulting in the fluorescence of CdS QDs in an “on” state. Importantly, the degree of fluorescence recovery of CdS QDs displayed a desirable linear correlation with the concentration of AA in the range of 5.0–100.0 $\mu\text{mol/L}$, the linear equation is $y = 0.0119c_{AA} + 0.3113$, and the detection limit is 1.16 $\mu\text{mol/L}$ ($S/N = 3, n = 9$). There was almost no interference with common amino acid, glucose and biological sulfhydryl small molecules to AA. Trace amount of AA in vitamin C tablets were determined and satisfactory results were obtained; the recoveries were observed to be 98.01–100.7%.

Keywords: CdS quantum dots; PDA; fluorescence resonance energy transfer; ascorbic acid



Citation: Li, P.; Chen, X.; Wu, G.; Wang, Z.; Huang, C. Ascorbic Acid Sensor Based on CdS QDs@PDA Fluorescence Resonance Energy Transfer. *Molecules* **2022**, *27*, 2097. <https://doi.org/10.3390/molecules27072097>

Academic Editor: Simone Morais

Received: 22 February 2022

Accepted: 20 March 2022

Published: 24 March 2022

Publisher's Note: MDPI stays neutral with regard to jurisdictional claims in published maps and institutional affiliations.



Copyright: © 2022 by the authors. Licensee MDPI, Basel, Switzerland. This article is an open access article distributed under the terms and conditions of the Creative Commons Attribution (CC BY) license (<https://creativecommons.org/licenses/by/4.0/>).

1. Introduction

The ascorbic acid (AA), a highly reductive polyhydroxy compound, is broadly used in the food industry as a source of vitamin C (Vc) or as an antioxidant, which acts as a key co-enzyme involved in a variety of indispensable biosynthetic processes such as amino acid metabolism, immune function, maintenance, non-heme iron absorption and so on in the human body [1–3]. Clinical trials have exhibited that AA supplementation produces antidepressant effects and improves mood [4]. However, as an essential nutrient that cannot be synthesized directly by the body, AA needs to be consumed from external foods and beverages. AA levels are associated with many diseases. Insufficient AA intake can lead to scurvy, while excessive AA intake can lead to kidney stones and stomach cramps [5,6]. Recent research has demonstrated the role of AA in stress-related disorders, inhibiting the development of cancer, and preventing and treating infection against COVID-19, making it urgent to analyze AA concentrations in food and clinical fields, especially for the performance measure of the techniques such as selectivity, sensitivity, and limit of detection in their utilization [4,7–10].

A range of analytical tools for the detection of AA have been proposed, including colorimetry [11–13], UV-vis spectrophotometry [14], electrochemical analysis [15–19], capillary electrophoresis [20,21], fluorescence analysis [22–24] and chromatography [25,26]. However, they are limited by the complexity of operations, low sensitivity or selectivity, expensive equipment, and time constraints. Electrochemical assay requires complex electrode modification procedures. Among them, the fluorescence method draws more attention owing to its high sensitivity, rapid response and operational simplicity, which makes for

more potential in AA detection. Thus, designing a simple and efficient sensor for AA detection is essential. A considerable number of assays based on the FRET have been presented. For example, Wu et al. designed carbon quantum dots as the FRET organophosphate pesticides determination [27]. Tian et al. presented a FRET aptasensor between nanoceria and graphene quantum dots for the determination of ochratoxin A [28].

Dopamine (DA) existing in the form of hydrochloride is a catecholamine neurotransmitter regulating many biological processes in the brain. Under alkaline conditions, it can be oxidized to dopamine quinone and self-polymerizes in aqueous solution to form a series of oligomers with different molecular weights, while dopamine, dopamine quinone and their oligomers self-assemble in solution to form assemblies of different structures through various non-covalent bonds, collectively referred to as polydopamine (PDA) [29]. PDA has been proven as a fluorescence-quenching agent with good dispersibility, stability in aqueous solution, a wide absorption spectrum and high extinction coefficient [30–34]. It is reported that the fluorescence of FITC-labeled ssDNA can be quenched by PDA to the fluorescence “off” state through FRET. However, the spontaneous oxidative polymerization reaction from DA to PDA would be blocked, leading to the fluorescence “on” state when there are various antioxidants [35,36].

As semiconductor nanoparticles, QDs have become a heated topic of research owing to their high quantum yield, broad absorption spectrum, tunable emission and high optical stability, as well as their good dispersion in aqueous solution and good biocompatibility [37–39]. Studies have shown that QDs have been applied to life science, semiconductor devices and other fields.

Hence, we developed a fluorescence “off-on” assay for AA by means of CdS QDs coupled with PDA-based FRET (Figure 1). CdS QDs can be assembled on the surface of PDA with strong affinity via the covalent interaction between -COOH of mercaptoacetic acid (TGA) and -NH₂ in the PDA, and then the fluorescence of CdS QDs (as a donor) was quenched by PDA (as an acceptor) to the “off” state via FRET, and the fluorescence-quenching mechanism between PDA and CdS QDs follows a dynamic, quenching mechanism that has been demonstrated. However, the oxidative polymerization of DA to produce PDA will be effectively suppressed and the quenching effect will be eliminated when AA exists. This is because AA can competitively terminate the spontaneous oxidative polymerization of dopamine by forming free radical cations through electron transfer, resulting in the fluorescence of CdS QDs’ recovery and being put in an “on” state [36,40].

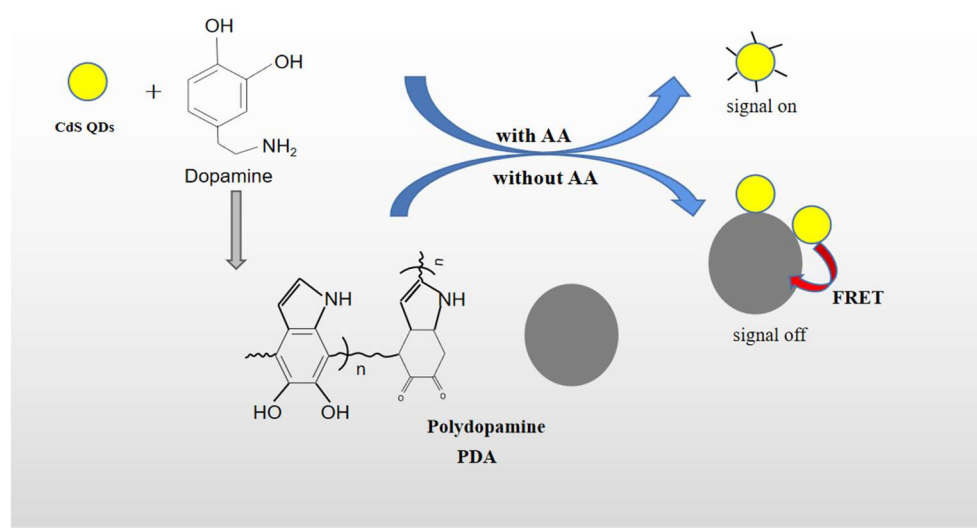


Figure 1. Construction principle of fluorescence signal “off” and “on” AA sensor.

2. Results and Discussion

2.1. Characterization

The following characterization was performed after centrifugation of CdS QDs with PDA and CdS QDs@PDA.

2.1.1. TEM Characterization

High-resolution TEM images of CdS QDs, PDA and CdS QDs@PDA are shown in Figure 2a–c. The results showed that CdS QDs, PDA and CdS QDs@PDA can be uniformly dispersed in water and the morphology were spherical or elliptical. Figure 2d–f exhibited their respective particle size distribution. It can be seen that the average particle size of CdS QDs, PDA and CdS QDs@PDA was about 3.2, 10.3 and 14.7 nm, respectively. Compared with CdS QDs and PDA, the particle size of CdS QDs@PDA was slightly larger, and the particle size distribution was more concentrated, which indirectly proved that CdS QDs was successfully assembled on the surface of PDA.

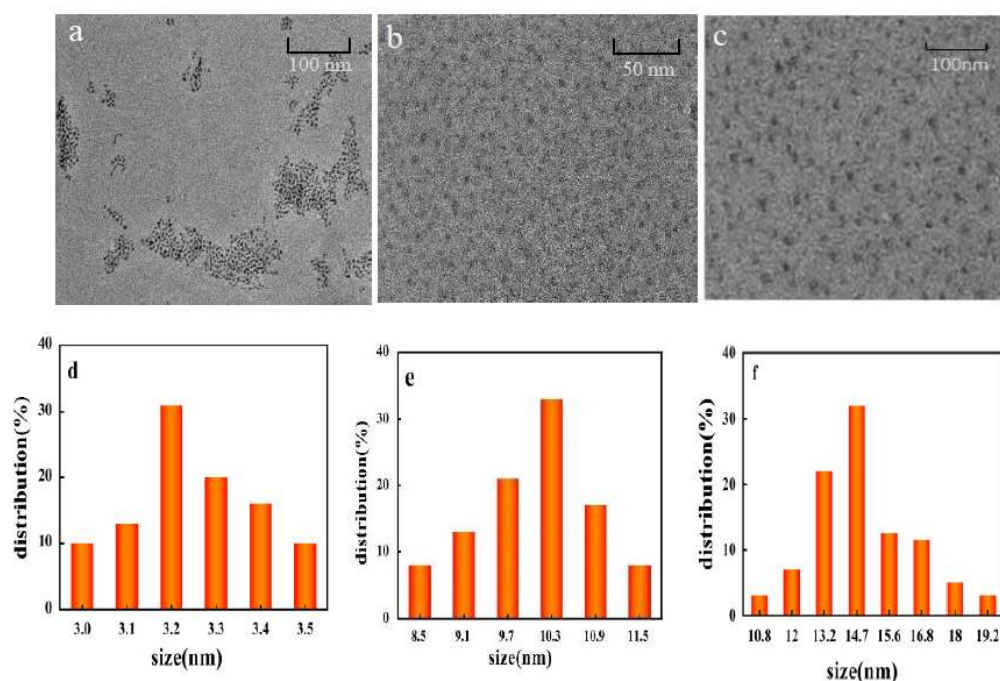


Figure 2. TEM images of CdS QDs (a), PDA (b) and CdS QDs@PDA (c). Particle size distribution of CdS QDs (d), PDA (e) and CdS QDs@PDA (f).

2.1.2. X-ray Photoelectron Spectroscopy (XPS) Characterization of CdS QDs and CdS QDs@PDA

Figure 3A showed XPS images of CdS QDs (a), CdS QDs@PDA (b) and analyzed their surface's chemical state. The peaks around 405, 160, 285, 404 and 530 eV that can be clearly observed represent the characteristic peaks of Cd 3d, S 2p, C 1s, N 1s and O 1s, respectively. The core-level XPS spectrum of O 1s (Figure 3B) exhibited three characteristic peaks at 532.38, 531.22 and 532.38 eV, which could be assigned to C-O, C=O and O-N bonds [41,42]. Figure 3C exhibited the high-resolution Cd 3d spectrum. The peaks at 411.34 and 404.58 eV are Cd 3d_{3/2} and Cd 3d_{5/2} diffraction peaks [43,44]. Figure 3D displayed the high-resolution S 2p spectrum which peaks at 162.10 eV and 161.07 eV, and can be ascribed to S 2p_{1/2} and S 2p_{3/2} [45,46], which belongs to C=S and Cd-S bond. High resolution C 1s spectrum (Figure 3E) could be deconvoluted into four characteristic peaks at 284.40, 285.80, 286.51 and 287.21 eV, which attributed to C-C, C-N, C-O and C=O bonds. The N 1s peaks (Figure 3F) at 404.35 and 404.89 eV could be associated with =N- and -NH₂ groups [42]. The results from XPS characterizations confirmed that CdS QDs have been assembled on PDA surface.

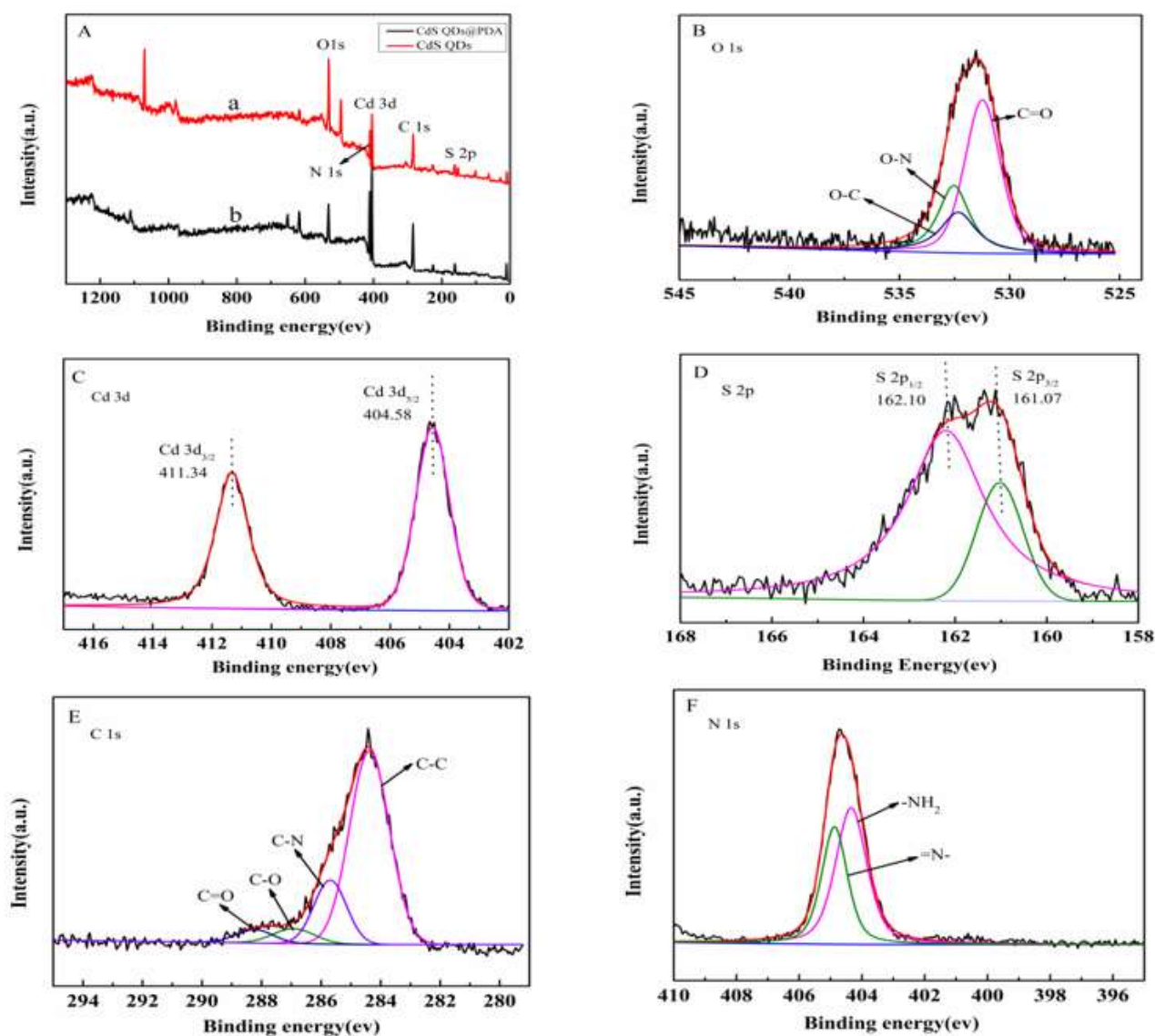


Figure 3. XPS spectrum (A) of CdS QDs (a) and CdS QDs@PDA (b). High resolution XPS spectra of O 1s (B), Cd 3d (C), S 2p (D), C 1s (E) and N 1s (F).

2.1.3. FTIR Characterization of DA and CdS QDs@PDA

As illustrated in Figure 4, the strong, stretching, vibration-absorption peaks of N-H and O-H bond were a wide peak of $3500\text{--}3100\text{ cm}^{-1}$, and the weak stretching vibration absorption peaks of C-H bond appeared at 2970 and 2885 cm^{-1} [47,48]. Compared with curve a, the absorption spectrum changed dramatically between 1700 and 500 cm^{-1} . The characteristic absorption peak of the DA molecule almost completely disappeared due to the generation of PDA and CdS QDs@PDA [49].

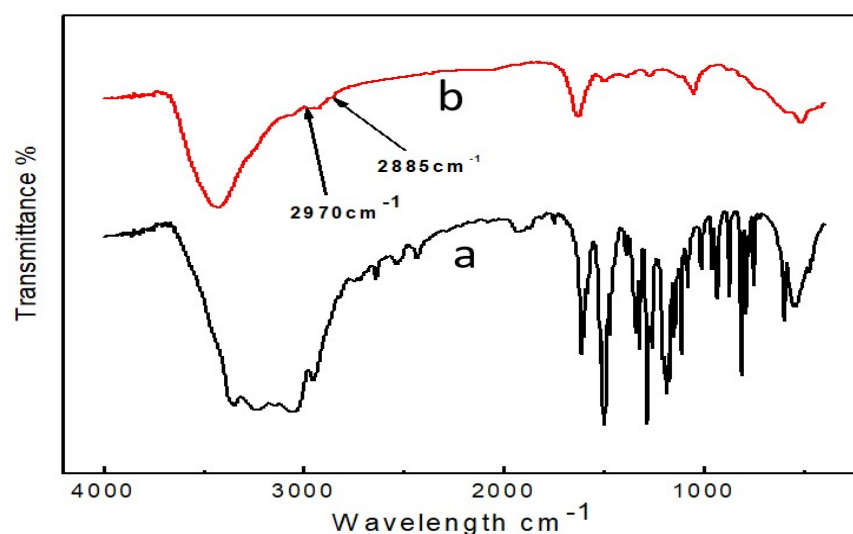


Figure 4. FTIR spectra of DA (a) and CdS QDs@PDA (b).

2.1.4. UV-Vis and Fluorescence Lifetime Characterization

Figure 5 displayed the absorption spectrum of PDA and the excitation and emission spectra of CdS QDs. It can be seen that the absorption spectrum of PDA was continuous between 300 and 800 nm, while the maximum excitation and emission wavelength of CdS QDs was near 445 and 593 nm. It was clear that the emission spectrum of the CdS QDs completely overlapped with the absorption spectrum of the PDA. The fluorescence quantum yield of CdS QDs was calculated to be about 2.4% using quinine sulfate (0.1 mol/L H₂SO₄) as the standard material. Additionally, the fluorescence lifetime of CdS QDs was significantly shorter in the presence of PDA than in its absence (Figure 6), indirectly proving the occurrence of FRET, which leads to fluorescence quenching of CdS QDs [50]. Therefore, the fluorescence quenching of CdS QDs by PDA followed the dynamic quenching mechanism.

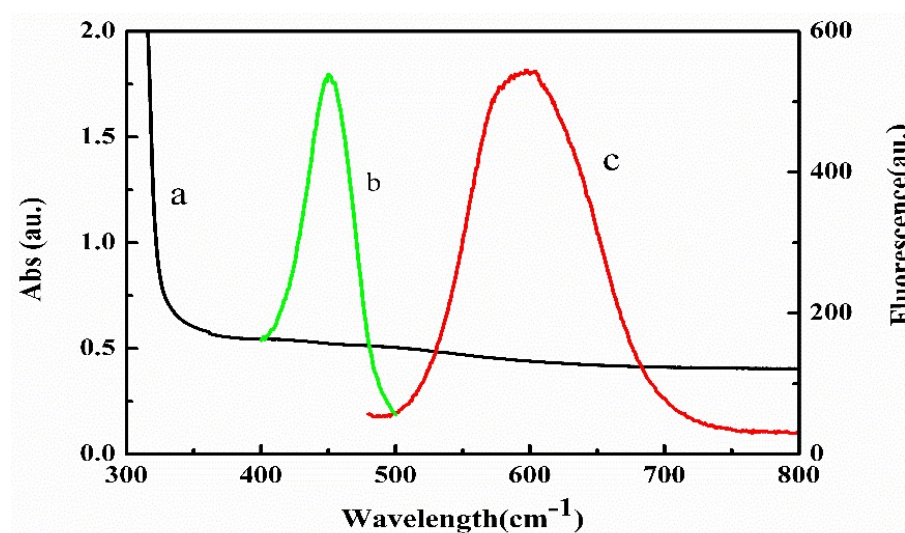


Figure 5. Absorption spectrum of PDA (a), excitation (b) and emission (c) spectra of CdS QDs.

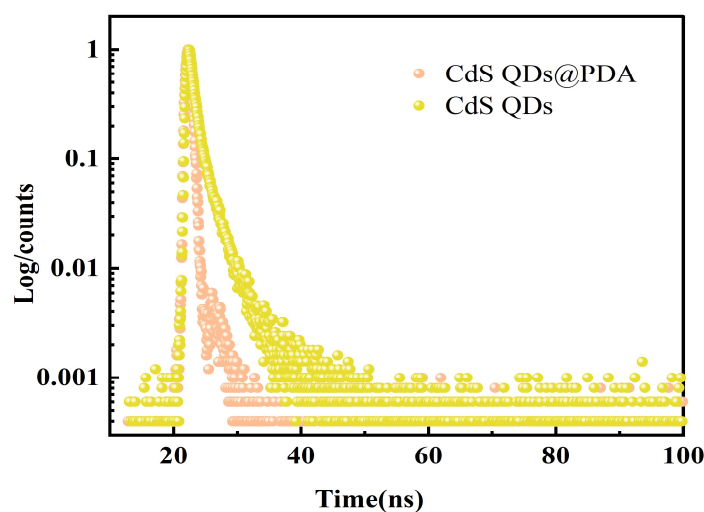


Figure 6. The luminescence time decay resolution curves of CdS QDs in the absence and presence of PDA (5 mmol/L DA).

2.2. Optimum Proposal

2.2.1. Study on Fluorescence Quenching and Recovery of CdS QDs

Figure 7a shows the effect of pH on the fluorescence emission of CdS QDs. The fluorescence intensity of CdS QDs was relatively stable when the pH was 6.0–8.0. When pH was below 6.0, the fluorescence intensity decreases, probably because the acid (H^+) could etch the surface S^{2-} to form HS^-/H_2S , which would generate surface defects [51]. When pH exceeded 8.0, it may be due to the difficulty of CdS QDs forming, or more defective CdS QDs forming at higher pH environments [52]. Figure 7b displayed the variation of recovery rate with pH. It can be seen that $(F - F_0)/F_0$ increases and then decreases rapidly with increasing pH (F and F_0 refer to the fluorescence intensities of CdS QDs in the presence and absence of AA, respectively), with the greatest $(F - F_0)/F_0$ at pH 6.5. This pH dependence may be related to the pK_a value of 4.10 for AA. At $pH > 4.10$, the ascorbic acid anion is the dominant species, and this anion readily precipitates stable radicals from resonance with a high reducing capacity, so that $(F - F_0)/F_0$ increases gradually with increasing pH in the range of 6.0–6.5. However, in neutral- and weakly basic solutions, AA is unstable and easily oxidized by dissolved oxygen. Thus, $(F - F_0)/F_0$ decreases rapidly with increasing pH in the range of 6.5–8.0 [53]. Therefore, 0.1 mol/L PBS at pH 6.5 was chosen throughout the reaction.

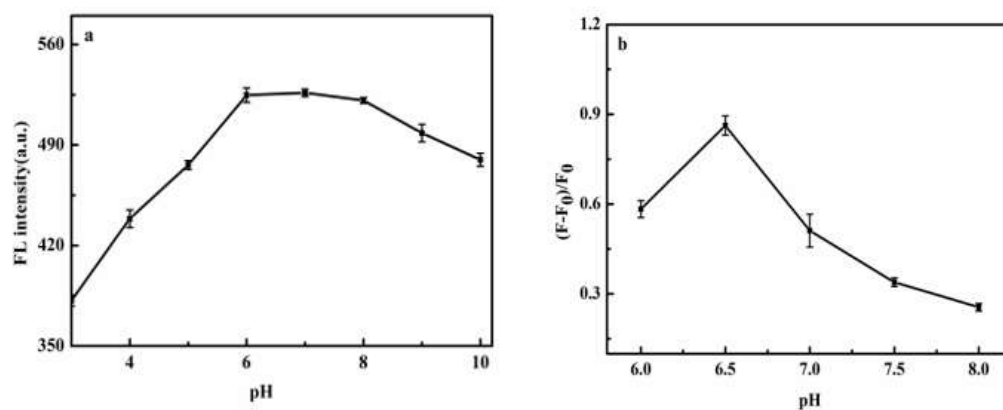


Figure 7. Effect of pH on fluorescence intensity of CdS QDs (a) and fluorescence quenching rate of CdS QDs by PDA (b).

2.2.2. Effect of DA Concentration and Reaction Time on Fluorescence Quenching of CdS QDs

Figure 8 exhibited that the fluorescence intensity of CdS QDs gradually decreased with the increase in DA concentration (a) and quenching reaction time (b). This was the enhancement of FRET due to an increase in the generated PDA with the increase in DA concentration [54]. When DA concentration was 5.0 mmol/L, and the reaction time reached 40 min, the fluorescence quenching rate tended to balance. Hence, for DA (5 mmol/L), the quenching reaction time of 40 min was selected for subsequent experiments.

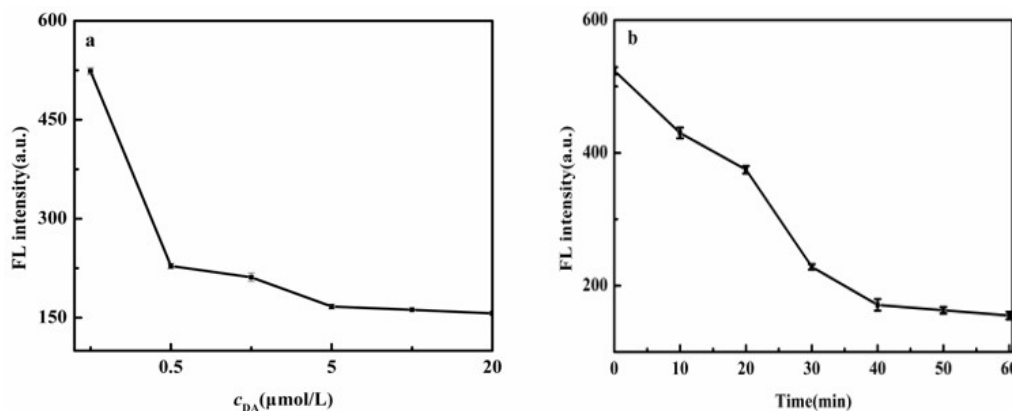


Figure 8. Effect of DA concentration (a) and quenching reaction time (b) on fluorescence intensity of CdS QDs.

2.3. Analysis Characteristics of Sensors

2.3.1. Linear Range and Detection Limits

The detection performance of CdS QDs@PDA for AA was further studied under the optimal conditions. As shown in Figure 9a, the fluorescence intensity of CdS QDs recovered gradually with the increase of AA concentration and the relationship between the fluorescence recovery rate of CdS QDs and AA concentration satisfied the following equation:

$$\frac{F - F_0}{F_0} = kc_{AA} + b \quad (k \text{ is the quenching constant})$$

As shown in Figure 9b, a good linear relationship was demonstrated with the concentration of AA in the range of 5.0 to 100.0 $\mu\text{mol/L}$. The linear equation was $y = 0.0119c_{AA} + 0.3113$ ($R^2 = 0.9959$) and the limit of detection (LOD) was 1.16 $\mu\text{mol/L}$ ($S/N = 3, n = 10$).

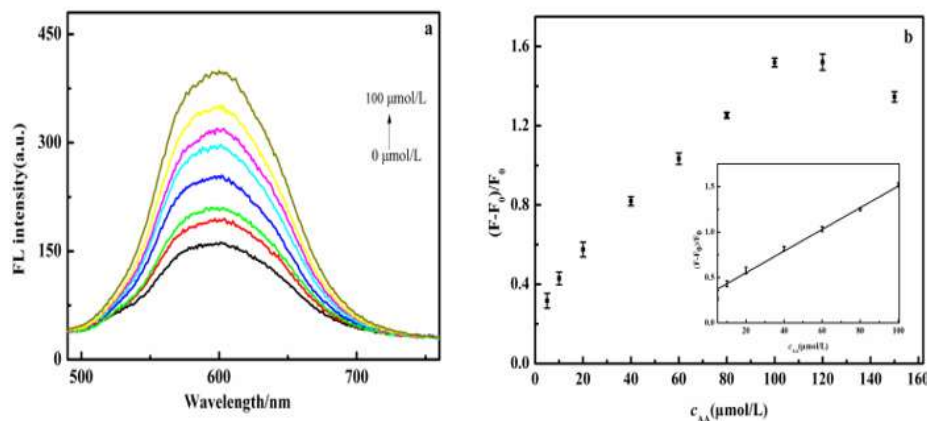


Figure 9. (a) Fluorescence spectra of sensor in the presence of different concentrations of AA. (b) Linear calibration curve for detection of AA.

2.3.2. Selectivity

To investigate the selectivity of the fluorescent sensor for AA, seventeen kinds of representative substances were selected for the interference test at a constant concentration of 100 $\mu\text{mol/L}$ (the same concentration as AA), including amino acid (Try, Ala, Tyr, Gly, Arg, Val, Cit, Asp, Leu, Phe, His, Met, Thr), bio-sulphydryl small molecules (MCE, D-PA, DTT) and glucose, and were added independently into the solution of CdS QDs. The results are illustrated in Figure 10. A strong fluorescence quenching was observed against AA but not on other individual interfering substances, demonstrating that the sensor has good immunity to interference when interfering substances co-exist. Thus, the sensor we designed had a better selectivity for AA.

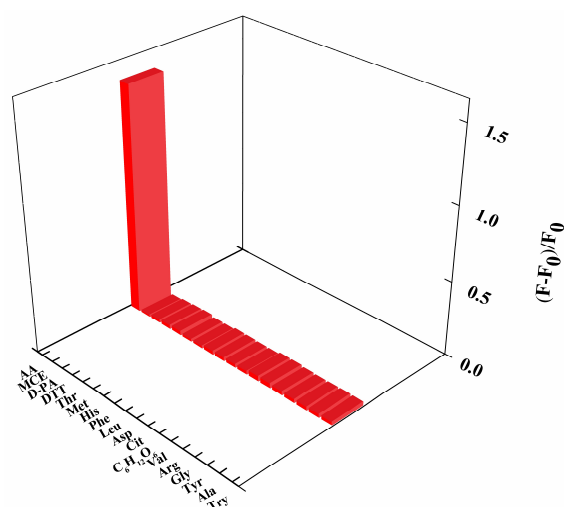


Figure 10. Selectivity of the proposed CdS QDs based fluorescent sensor for AA detection.

2.3.3. Actual Sample Analysis and Recovery

As can be seen from Table 1, the determination of AA in vitamin C tablets by this method was basically consistent with the labeled amount (0.1 g). The recoveries were observed to be 98.01–100.7%.

Table 1. The content and recovery of AA in vitamin C tablets samples.

Sample	Labeled (g/Piece)	Detected/ $\mu\text{mol}\cdot\text{L}^{-1}$ ($x \pm SD, n = 3$)	Added / $\mu\text{mol/L}$	Found/ $\mu\text{mol/L}$ ($x \pm SD, n = 3$)	Recovery/% ($x \pm SD, n = 3$)
Vc tables	0.1	7.28 ± 0.61	7.50	14.63 ± 0.11	98.01 ± 1.47
		20.23 ± 0.80	20.00	40.19 ± 0.81	100.7 ± 1.55
		40.88 ± 1.68	40.00	80.46 ± 1.05	99.01 ± 2.60

3. Experiment

3.1. Material and Reagents

Alanine (Ala), Glycine (Gly), Arginine (Arg), Tryptophane (Try), Valine (Val), Tyrosine (Tyr), Citrulline (Cit), Aspartic acid (Asp), Leucine (Leu), Phenylalanine (Phe), Threonine (Thr), Histidine (His), Methionine (Met), Dithiothreitol (DTT), Dopamine (DA), D-penicillamine (D-PA), Ascorbic acid (AA), Chromic chloride (CdCl_2) and Sodium sulfide (Na_2S) were purchased from Aladdin Co., Ltd., Shanghai, China; 2-mercaptoethanol (MCE), Glucose ($\text{C}_6\text{H}_{12}\text{O}_6$) and Sodium hydroxide (NaOH) were obtained from Sinopharm Chemical Reagent Co., Ltd., Shanghai, China; Mercaptoacetic acid (TGA) was supplied by Sigma-Aldrich Co., Ltd., St. Louis, MO, USA; Tris hydrochloride (Tris-HCl) was acquired from Adamas reagent Co., Ltd., Shanghai, China; vitamin tablets were purchased from Huazhong Pharmaceutical Co., Ltd., Xiangyang, China; the experimental water was ultrapure water.

3.2. Apparatus

The UV-vis absorption spectra were carried out using Lambda 950 spectrophotometer (PerkinElmer Inc., Waltham, MA, USA). The surface morphology of the prepared materials was characterized via S-4800 Scanning Electron Microscope (JEOL, Zaventem, Belgium). The X-ray photoelectron spectrometer was conducted on ESCALAB 250Xi X-ray photoelectron spectroscopy (Reonicolai Inc., New York, NY, USA). The FT-IR spectra was recorded on Thermo Nexus 670 infrared spectrometer (Reonicolai Inc., New York, NY, USA). Fluorescence (FL) spectra were performed on RF-6000 Fluorescence Spectrometer (Shimadzu, Kyoto, Japan). Fluorescence lifetime spectra are determined by FLS 980 Fluorescence Spectrometer (Tenmei, Edinburgh, UK). Plus-E3-20TH Ultrapure Water Device (Nioelet, MN, USA). PHS-3C pH meter (Shanghai Yidian Scientific Instrument Co., Ltd., Shanghai, China), 1810D Electronic Analytical Balance (Saidoris, Baden-Württemberg, Germany).

3.3. Synthesis of CdS QDs

CdS QDs was synthesized as previously reported [55]. In total, 50 mL 0.01 mol/L CdCl₂ and 250 µL TGA were added to a 150 mL tri-neck flask. The pH was set to 11.0 using NaOH solution (1 mol/L), and oxygen was removed through N₂ for 30 min. Then, 5.0 mL 0.1 mol/L Na₂S solution was added before restarting the flow at 100 °C for 4 h under the protection of nitrogen. CdS QDs was obtained and kept at 4 °C for further use.

3.4. Optimization of Fluorescence Quenching Conditions

In total, 200 µL of CdS QDs were added to 2 mL centrifuge tubes, diluted and fixed with a pH of 3.0, 4.0, 5.0, 6.0, 7.0, 8.0, 9.0 and 10.0 buffer solution. Fluorescence was measured to determine the optimal emission pH range of CdS QDs and select the buffer system. Different concentrations of DA were then added simultaneously to select the optimum quenching pH, DA concentration and sonication reaction time.

3.5. Determination of Ascorbic Acid

CdS QDs (200 µL) were mixed with a series of aqueous solution of AA at different concentrations. DA (5 mmol/L) was added to the mixture and diluted with a phosphate buffer (pH = 6.5, 0.1 mol/L) to 2 mL (the final concentration of AA was 0.00, 5.00, 10.0, 20.0, 40.0, 60.0, 80.0, 100.0, 120.0 and 150.0 µmol/L). The fluorescence intensity was determined with the excitation wavelength of 445 nm after 40 min of ultrasonic reaction.

3.6. Actual Sample Handling

Vc tablets were measured using the same method as the actual samples. The mass of each tablet was obtained by accurately weighing 100 pieces of Vc and ground into powder. Vc powder of a certain quality was accurately weighed, dissolved in water to a certain volume and filtered. The filtrate was diluted step by step to the appropriate concentration for determination.

4. Conclusions

An “off” and “on” fluorescence sensing platform was constructed for the sensitive detection of AA based on the FRET between CdS QDs and PDA. The sensitive and rapid detection of AA in Vc tablets were successfully achieved. It can be foreseen that this technique can be extended to the determination of AA in other samples. At the same time, different signal sources can be used to construct a new sensor with PDA to realize the detection of various reductants.

Author Contributions: Conceptualization, P.L., X.C. and C.H.; methodology, P.L., X.C., G.W. and Z.W.; data curation, P.L., X.C., G.W. and Z.W.; formal analysis, P.L. and C.H.; writing—original draft, P.L.; writing—review and editing, C.H. All authors have read and agreed to the published version of the manuscript.

Funding: The authors gratefully acknowledge the support for this research from the National Natural Science Foundation of China (21575129).

Institutional Review Board Statement: Not applicable.

Informed Consent Statement: Not applicable.

Data Availability Statement: Not applicable.

Conflicts of Interest: The authors have no conflict of interest to declare.

Sample Availability: Samples of the compounds in this article are not available from the author.

References

1. Zhai, C.; Hou, B.; Peng, P.; Zhang, P.; Chen, X. Hydrogen bonding interaction of ascorbic acid with nicotinamide: Experimental and theoretical study. *J. Mol. Liq.* **2018**, *249*, 9–15.
2. Rao, H.; Ge, H.; Lu, Z.; Liu, W.; Chen, Z.; Zhang, Z.; Wang, X.; Zou, P.; Wang, Y.; He, H. Copper nanoclusters as an on-off-on fluorescent probe for ascorbic acid. *Microchim. Acta* **2016**, *183*, 1651–1657.
3. Wei, Z.; Li, H.; Liu, S.; Wang, W.; Chen, H.; Xiao, L. Carbon Dots as Fluorescent/Colorimetric Probes for Real-Time Detection of Hypochlorite and Ascorbic Acid in Cells and Body Fluid. *Anal. Chem* **2019**, *91*, 15477–15483.
4. Moritz, B.; Schmitz, A.E.; Rodrigues, A.; Dafre, A.L.; Cunha, M.P. The role of vitamin C in stress-related disorders. *J. Nutr. Biochem.* **2020**, *85*, 108459. [PubMed]
5. Zuo, X.; Zhang, H.; Li, N. An electrochemical biosensor for determination of ascorbic acid by cobalt (II) phthalocyanine–multi-walled carbon nanotubes modified glassy carbon electrode. *Sens. Actuators B Chem.* **2012**, *161*, 1074–1079.
6. Ma, F.; Luo, J.; Li, X.; Liu, S.; Chen, X. A “switch-on” fluorescence assay based on silicon quantum dots for Determination of Ascorbic Acid. *Spectrochim. Acta. A Mol. Biomol. Spectrosc.* **2021**, *249*, 119343.
7. Kumari, A.; Vyas, V.; Kumar, S. Advances in electrochemical and optical sensing techniques for vitamins detection: A review. *ISSS J. Micro Smart Syst.* **2021**, *463*, 1–13.
8. Reang, J.; Sharma, P.C.; Thakur, V.K.; Majeed, J. Understanding the Therapeutic Potential of Ascorbic Acid in the Battle to Overcome Cancer. *Biomolecules* **2021**, *11*, 1130.
9. Hoang, X.; Shaw, G.; Fang, W.; Han, B. Possible Application of High Dose Vitamin C in the Prevention and Therapy for Coronavirus Infections. *J. Glob. Antimicrob. Resist.* **2020**, *23*, 256–262.
10. Capponi, P.C.; Murri, D.; Pernice, C. Topical L-Ascorbic Acid Formulation for a Better Management of Non-Melanoma Skin Cancer: Perspective for Treatment Strategies. *Pharmaceutics* **2021**, *13*, 1201.
11. Jun, P.; Ling, J.; Zhang, X.Q.; Zhang, L.Y.; Cao, Q.E.; Ding, Z.T. A rapid, sensitive and selective colorimetric method for detection of ascorbic acid. *Sens. Actuators B Chem.* **2015**, *221*, 708–716.
12. Yang, Q.; Wang, X.; Peng, H.; Arabi, M.; Chen, L. Ratiometric fluorescence and colorimetry dual-mode assay based on manganese dioxide nanosheets for visual detection of alkaline phosphatase activity. *Sens. Actuators B Chem.* **2020**, *302*, 127176.
13. Chen, J.; Ge, J.; Zhang, L.; Li, Z.; Sun, Y.; Qu, L. Reduced graphene oxide nanosheets functionalized with poly (styrene sulfonate) as a peroxidase mimetic in a colorimetric assay for ascorbic acid. *Microchim. Acta* **2016**, *183*, 1847–1853.
14. Aguilar, K.; Garvin, A.; Lara-Sagahon, A.V.; Ibarz, A. Ascorbic acid degradation in aqueous solution during UV-Vis irradiation. *Food Chem.* **2019**, *297*, 124864.
15. Cheng, H.; Wang, X.; Wei, H. Ratiometric Electrochemical Sensor for Effective and Reliable Detection of Ascorbic Acid in Living Brains. *Anal. Chem.* **2015**, *87*, 8889–8895.
16. Jirimali, H.D.; Nagarale, R.K.; Saravanakumar, D.; Lee, J.M.; Shin, W. Hydroquinone modified chitosan/carbon film electrode for the selective detection of ascorbic acid. *Carbohydr. Polym.* **2013**, *92*, 641–644.
17. Liu, K.; Yu, P.; Lin, Y.; Wang, Y.; Ohsaka, T.; Mao, L. Online electrochemical monitoring of dynamic change of hippocampal ascorbate: Toward a platform for in vivo evaluation of antioxidant neuroprotective efficiency against cerebral ischemia injury. *Anal. Chem.* **2013**, *85*, 9947–9954.
18. Wu, F.; Huang, T.; Hu, Y.; Yang, X.; Ouyang, Y.; Xie, Q. Differential pulse voltammetric simultaneous determination of ascorbic acid, dopamine and uric acid on a glassy carbon electrode modified with electroreduced graphene oxide and imidazolium groups. *Microchim. Acta* **2016**, *183*, 2539–2546.
19. Dhara, K.; Mahapatra, D.R. Review on nanomaterials-enabled electrochemical sensors for ascorbic acid detection. *Anal. Biochem.* **2019**, *586*, 113415.
20. Kim, W.S.; Dahlgren, R.L.; Moroz, L.L.; Sweedler, J.V. Ascorbic acid assays of individual neurons and neuronal tissues using capillary electrophoresis with laser-induced fluorescence detection. *Anal. Chem.* **2002**, *74*, 5614–5620.
21. Neuberger, S.; Jooß, K.; Flottmann, D.; Scriba, G.; Neusüß, C. Raman spectroscopy and capillary zone electrophoresis for the analysis of degradation processes in commercial effervescent tablets containing acetylsalicylic acid and ascorbic acid. *J. Pharm. Biomed. Anal.* **2017**, *134*, 122–129. [PubMed]
22. Wang, Y.; Yang, Y.; Liu, W.; Ding, F.; Zou, P.; Wang, X.; Zhao, Q.; Rao, H. A carbon dot-based ratiometric fluorometric and colorimetric method for determination of ascorbic acid and of the activity of ascorbic acid oxidase. *Microchim. Acta* **2019**, *186*, 246.

23. Liu, S.; Pang, S. A dual-model strategy for fluorometric determination of ascorbic acid and of ascorbic acid oxidase activity by using DNA-templated gold-silver nanoclusters. *Microchim. Acta* **2018**, *185*, 426.
24. Li, N.; Li, Y.; Han, Y.; Pan, W.; Zhang, T.; Tang, B. A Highly Selective and Instantaneous Nanoprobe for Detection and Imaging of Ascorbic Acid in Living Cells and in Vivo. *Anal. Chem.* **2014**, *86*, 3924–3930.
25. Garnero, C.; Longhi, M. Development of HPLC and UV spectrophotometric methods for the determination of ascorbic acid using hydroxypropyl- β -cyclodextrin and triethanolamine as photostabilizing agents. *Anal. Chim. Acta* **2010**, *659*, 159–166.
26. Wang, S.; Schram, I.M.; Sund, R.B. Determination of plasma ascorbic acid by HPLC: Method and stability studies. *Eur. J. Pharm. Sci.* **1995**, *3*, 231–239.
27. Wu, X.; Song, Y.; Yan, X.; Zhu, C.; Ma, Y.; Du, D.; Lin, Y. Carbon quantum dots as fluorescence resonance energy transfer sensors for organophosphate pesticides determination. *Biosens. Bioelectron.* **2017**, *94*, 292–297.
28. Tian, J.; Wei, W.; Wang, J.; Ji, S.; Chen, G.; Lu, J. Fluorescence resonance energy transfer aptasensor between nanoceria and graphene quantum dots for the determination of ochratoxin A. *Anal. Chim. Acta* **2018**, *1000*, 265–272.
29. Batul, R.; Tamanna, T.; Khaliq, A.; Yu, A. Recent progress in the biomedical applications of polydopamine nanostructures. *Biomater. Sci.* **2017**, *5*, 1204–1229.
30. Yan, J.; Yang, L.; Lin, M.F.; Ma, J.; Lu, X.; Lee, P.S. Polydopamine Spheres as Active Templates for Convenient Synthesis of Various Nanostructures. *Small* **2013**, *9*, 596–603.
31. Ju, K.Y.; Lee, Y.; Lee, S.; Park, S.B.; Lee, J.K. Bioinspired Polymerization of Dopamine to Generate Melanin-Like Nanoparticles Having an Excellent Free-Radical-Scavenging Property. *Biomacromolecules* **2011**, *12*, 625–632. [[PubMed](#)]
32. Ji, X.; Yi, B.; Xu, Y.; Zhao, Y.; Zhong, H.; Ding, C. A Novel Fluorescent Biosensor for Adenosine Triphosphate Detection Based on the polydopamine nanospheres integrating with enzymatic recycling amplification. *Talanta* **2017**, *169*, 8–12. [[PubMed](#)]
33. Choi, C.K.K.; Li, J.; Wei, K.; Xu, Y.J.; Ho, L.W.C.; Zhu, M.; To, K.K.W.; Choi, C.H.J.; Bian, L. A Gold@ Polydopamine Core-Shell Nanoprobe for Long-Term Intracellular Detection of MicroRNAs in Differentiating Stem Cells. *J. Am. Chem. Soc.* **2015**, *137*, 7337–7346. [[PubMed](#)]
34. Qiang, W.; Hu, H.; Sun, L.; Li, H.; Xu, D. Aptamer/Polydopamine Nanospheres Nanocomplex for in Situ Molecular Sensing in Living Cells. *Anal. Chem.* **2015**, *87*, 12190–12196.
35. Ma, S.; Qi, Y.X.; Jiang, X.Q.; Chen, J.Q.; Zhou, Q.Y.; Shi, G.; Zhang, M. Selective and sensitive monitoring of cerebral antioxidants based on the dye-labeled DNA/polydopamine conjugates. *Anal. Chem.* **2016**, *88*, 11647–11653.
36. Zhu, S.; Yan, X.; Qiu, J.; Sun, J.; Zhao, X.E. Turn-on fluorescent assay for antioxidants based on their inhibiting polymerization of dopamine on graphene quantum dots. *Spectrochim. Acta. A Mol. Biomol. Spectrosc.* **2020**, *225*, 117516.
37. Khaledian, S.; Nalaini, F.; Mehrbakhsh, M.; Abdoli, M.; Zahabi, S.S. Applications of novel quantum dots derived from layered materials in Cancer cell imaging. *FlatChem* **2021**, *27*, 100246.
38. Alivisatos, A.P.; Gu, W.; Larabell, C. Quantum Dots as Cellular Probes. *Annu. Rev. Biomed. Eng.* **2005**, *7*, 55–76.
39. Kwonbeen, K.; Jongsung, K. Synthesis of Carbon Quantum Dots from Jujubes for Detection of Iron (III) Ions. *J. Nanosci Nanotechnol.* **2018**, *18*, 1320–1322.
40. Zhao, Y.Y.; Li, L.; Yu, R.Q.; Chen, T.T.; Chu, X. CoOOH-induced synthesis of fluorescent polydopamine nanoparticles for the detection of ascorbic acid. *Anal. Methods* **2017**, *9*, 5518–5524.
41. Song, T.; Zhu, X.; Zhou, S.; Yang, G.; Gan, W.; Yuan, Q. DNA derived fluorescent bio-dots for sensitive detection of mercury and silver ions in aqueous solution. *Appl. Surf. Sci.* **2015**, *347*, 505–513.
42. Li, Q.; Zhang, L.; Bai, J.; Liu, Z.; Liang, R.; Qiu, J. Preparation of novel fluorescent DNA bio-dots and their application for biothiols and glutathione reductase activity detection. *Biosens. Bioelectron.* **2015**, *74*, 886–894. [[PubMed](#)]
43. Wang, M.; Cui, Z.; Yang, M.; Lin, L.; Chen, X. Core/shell structured CdS/polydopamine/TiO₂ ternary hybrids as highly active visible-light photocatalysis. *J. Colloid Interface Sci.* **2019**, *544*, 1–7.
44. Lu, X.H.; Xie, S.L.; Zhai, T.; Zhao, Y.F.; Zhang, P.; Zhang, Y.L.; Tong, Y.X. Monodisperse CeO₂/CdS heterostructured spheres: One-pot synthesis and enhanced photocatalytic hydrogen activity. *RSC Adv.* **2011**, *1*, 1207–1210.
45. Souza, V.S.; Manjunath, K.; Ramakrishnappa, T.; Santos, J.M. Superior activity of the CuS-TiO₂/Pt hybrid nanostructure towards visible light induced hydrogen production. *New J. Chem.* **2016**, *40*, 10172–10180.
46. Chen, T.; Song, C.; Fan, M.; Hong, Y.; Hu, B.; Yu, L.; Shi, W. In-situ fabrication of CuS/g-C₃N₄ nanocomposites with enhanced photocatalytic H₂-production activity via photoinduced interfacial charge transfer. *Int. J. Hydrogen Energy* **2017**, *42*, 12210–12219.
47. Arvand, M.; Aazam, A.; Mirroshandel. An efficient fluorescence resonance energy transfer system from quantum dots to graphene oxide nano sheets: Application in a photoluminescence aptasensing probe for the sensitive detection of diazinon. *Food Chem.* **2019**, *280*, 115–122.
48. Kalajahi, S.T.; Rasekh, B.; Yazdian, F.; Neshati, J.; Taghavi, L. Green mitigation of microbial corrosion by copper nanoparticles doped carbon quantum dots nanohybrid. *Environ. Sci. Pollut. Res.* **2020**, *27*, 40537–40551.
49. Sharma, V.V.; Guadagnini, L.; Giorgetti, M.; Tonelli, D. Electrocatalytic determination of thiols using hybrid copper cobalt hexacyanoferrate modified glassy carbon electrode. *Sens. Actuators B Chem.* **2016**, *228*, 16–24.
50. Wang, M.; Wang, S.; Su, D.; Su, X. Copper nanoclusters/polydopamine nanospheres based fluorescence aptasensor for protein kinase activity determination. *Anal. Chim. Acta* **2018**, *1035*, 184–191.
51. Zhu, Y.; Li, Z.; Chen, M.; Cooper, H.M.; Lu, G.Q.; Xu, Z.P. One-pot preparation of highly fluorescent cadmium telluride/cadmium sulfide quantum dots under neutral-pH condition for biological application. *J. Colloid Interface Sci.* **2013**, *390*, 3–10. [[PubMed](#)]

52. Song, X.F.; Wang, W.; Yang, J.Y.; Li, T.T.; Liu, Y. Novel in-situ radiation construction of thioglycollic acid capped CdS quantum dots functionalized g-C₃N₄ nano hybrids with superior photocatalytic activity under visible light. *Radiat. Phys. Chem.* **2019**, *165*, 108449.
53. Gao, Y.; Yan, X.; Li, M.; Gao, H.; Wang, H. A “turn-on” fluorescence sensor for ascorbic acid based on graphene quantum dots via fluorescence resonance energy transfer. *Anal. Methods* **2018**, *10*, 611–616.
54. Chi, M.; Zhu, Y.; Jing, L.; Wang, C.; Lu, X. Fabrication of ternary MoS₂-polypyrrole-Pd nanotubes as peroxidase mimics with a synergistic effect and their sensitive colorimetric detection of l-cysteine. *Anal. Chim. Acta* **2018**, *1035*, 146–153.
55. Wang, G.L.; Xu, J.J.; Chen, H.Y. Selective detection of trace amount of Cu²⁺ using semiconductor nanoparticles in photoelectrochemical analysis. *Nanoscale* **2010**, *2*, 1112–1114.